Electronic Supplementary Material (ESI) for Materials Chemistry Frontiers.
This journal is © the Partner Organisations 2021

Supplementary Information

Ternary $NiTiO_3$@g-C_3N_4-Au nanofibers with synergistic Z-scheme core@shell interface and dispersive Schottky contact surface for enhanced solar photocatalytic activity

Jie Liu, Xinghua Li*, Chaohan Han, Xuejiao Zhou, Xiaowei Li, Yuan Liang, Shuai Liu, Changlu Shao* and Yichun Liu

Center for Advanced Optoelectronic Functional Materials Research, and Key Laboratory of UV Light-Emitting Materials and Technology of Ministry of Education, Northeast Normal University, 5268 Renmin Street, Changchun 130024, People's Republic of China

*Corresponding author:

Email: clshao@nenu.edu.cn; Tel. 8643185098803

Email: lixh781@nenu.edu.cn; Tel. 8643185098803

1. Experiments

1.1 Characterizations

Scanning electron microscopy (SEM) (Quanta 250 FEG XL-30) and transmission electron microscopy (TEM) (JEOL JEM-2100F) were used to observe morphologies of the samples. EDX (Energy-dispersive X-ray) spectroscope was used to analyze the elemental composition of the sample. The crystal structures of the samples were determined by X-ray diffraction (XRD) patterns, which was measured with a D/max 2500 XRD spectrometer (Rigaku, Japan). The scanning step of this instrument was 0.02 degree, while the testing range was 10 degrees to 80 degrees. UV-visible diffuse reflection spectra (DRS) in the range of 300–800 nm was measured by using UH4150 UV-Vis-NIR spectrophotometer with $BaSO_4$ as a reference. The surface elements and chemical states of samples were characterized using X-ray photoelectron spectroscopy (XPS) instrument (ESCALAB 250Xi) with an Mg Kα ($h\upsilon$ = 1253.6 eV) radiation source at a residual gas pressure of below 10^{-8} Pa and the location of calibrated carbon is 284.6 eV. Brunauer-Emmett-Teller (BET) instrument (Micromeritics ASAP2020) method was used to analyze the specific surface areas of the samples. SDT Q600 TG-DSC thermos-analyzer was used to investigate the loading contents of g-C_3N_4 on oxide nanofibers.

1.2 Photocatalytic testing

Photodegradation tests:

A 150 W Xe lamp (CEL-HXF300, Beijing CEL technology Co. Ltd.) coupled with an Am 1.5 cutoff filter was used as the simulated solar source for photocatalytic activity

tests. The degradations of rhodamine B (RhB) were performed with an initial concentration of 10 mg/L. 50.0 mg $NiTiO_3$@g-C_3N_4-Au NFs, 50.0 mg $NiTiO_3$@g-C_3N_4 NFs, 50.0 mg $NiTiO_3$ NFs, 35.0 mg g-C_3N_4 were dispersed into the solution with a volume of 50 mL. The solution was magnetically stirred in the dark for 30 min to reach adsorption equilibrium before illumination. During light irradiation, the flow of cooling water maintained the entire reaction system at room temperature. 2 mL filtrate was taken out of the solution every 20 min and analyzed by UV2600 UV-Vis-NIR spectrophotometer record the absorbance at 553 nm.

Hydrogen evolution tests:

A 150 W Xe lamp (CEL-HXF300, Beijing CEL technology Co. Ltd.) coupled with an Am 1.5 cutoff filter was used as the simulated solar source. 50.0 mg samples were suspended in a 100 mL mixed solution of methanol (10 mL) and distilled water (90 mL), then $H_2PtCl_6 \cdot 6H_2O$ alcohol solution (50 $g \cdot L^{-1}$) were added 8 uL of into above system. Before the photocatalytic experiment, a vacuum pump was used to remove the dissolved air of the entire reaction system completely. The reaction system was maintained at room temperature using a flow of cooling water. After this process, turn off the vacuum pump and start the analysis, the generated gases were analyzed with an on-line TCD gas chromatograph (CEL, GC-9720, N_2 carrier).

1.3 Photocurrent measurement

Photocurrents were measured on an electrochemical workstation (CHI660E, Shanghai Chenghua Instruments). The traditional three-electrode working system was used to measure photocurrent, the platinum net and a Hg_2SO_4 electrode (saturated KCl)

were used to counter electrode and reference electrode, respectively. 3 mg samples were dissolved in 0.1 ml anhydrous alcohol, grated in a mortar, evenly coated on an FTO glass of 1cm×1cm, dried at 60 °C for 30 min, and calcined in a tube furnace annealing at 250 °C for holding 1 hour. The electrolyte was Na_2SO_4 (0.2 M) aqueous solution.

1.4 Radical trapping experiments

During the photocatalysis process, 1.0 mg benzoquinone (BQ), 1ml tert-butyl alcohol (TBA), 1.0g $Pb(CH_3COO)_4$ and 50.0 mg ammonium oxalate (AO) were involved in RhB solutions, respectively. The BQ, TBA, $Pb(CH_3COO)_4$, and AO were used to captured the active species of superoxide radicals ($•O^{2-}$), hydroxyl radicals(•OH) and photogenerated electrons (e^-) and holes (h^+), respectively. All processes were the same as photocatalytic degradation of RhB. 2 ml filtrate was taken out of the solution every 20 min and analyzed by UV2600 UV-Vis-NIR spectrophotometer.

2. Supporting Figures

Figure captions of supporting figures

Fig.S1. Diameter distribution diagram of $NiTiO_3$@g-C_3N_4-Au NFs.

Fig.S2. EDX pattern of the ternary $NiTiO_3$@g-C_3N_4-Au NFs; the inset shows the atomic ratio of elements.

Fig.S3. SEM image of (A) pure g-C_3N_4 and (B) g-C_3N_4-Au.

Fig.S4. TGA curves of the binary $NiTiO_3$@g-C_3N_4 NFs and ternary $NiTiO_3$@g-C_3N_4-Au NFs

Fig.S5. BET Nitrogen adsorption/desorption isotherms of $NiTiO_3$ NFs, binary $NiTiO_3$@g-C_3N_4 NFs, ternary $NiTiO_3$@g-C_3N_4-Au NFs, and pure g-C_3N_4; the inset shows the BET specific surface area and pore volume of samples.

Fig.S6. (A) Fully scanned XPS spectra for the $NiTiO_3$ NFs, $NiTiO_3$@g-C_3N_4 NFs, $NiTiO_3$@g-C_3N_4-Au NFs and pure g-C_3N_4; (B) high-resolution XPS spectra of Au 4f for $NiTiO_3$@g-C_3N_4 NFs-Au NFs; (C) high-resolution XPS spectra of Ti 2p for $NiTiO_3$ NFs.

Fig.S7. Adsorption properties of different samples on RhB in the dark.

Fig.S8. Photocatalytic degradation of RhB for pure g-C_3N_4 under different pH environment HCl (pH = 3) and KOH (pH = 11) solution.

Fig.S9. EPR spectra of $NiTiO_3$@g-C_3N_4 NFs in the dark and light.

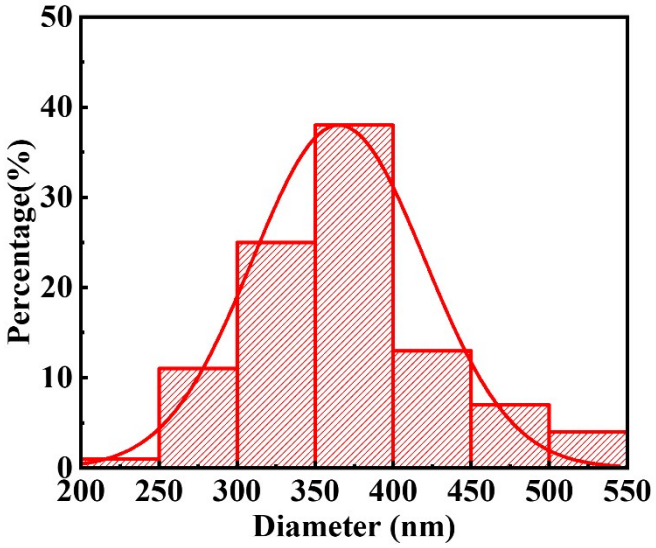

Fig.S1. Diameter distribution diagram of $NiTiO_3$@g-C_3N_4-Au NFs.

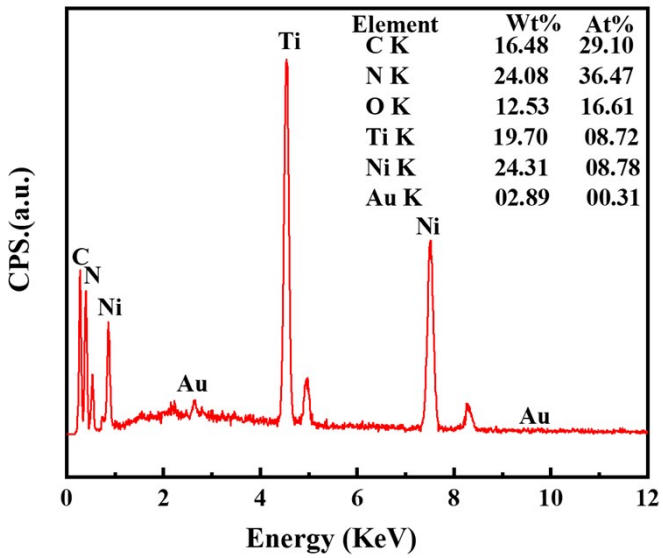

Fig.S2. EDX pattern of the ternary $NiTiO_3$@g-C_3N_4-Au NFs; the inset shows the atomic ratio of elements.

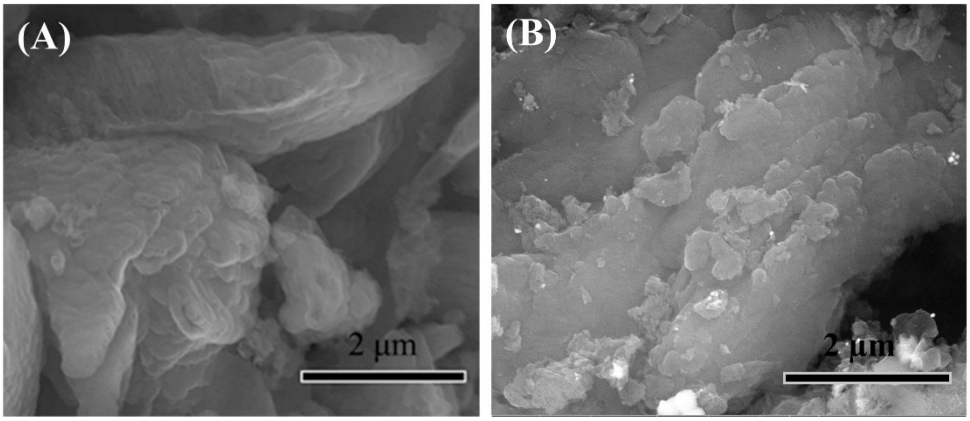

Fig.S3. SEM image of (A) pure g-C_3N_4 and (B) g-C_3N_4-Au.

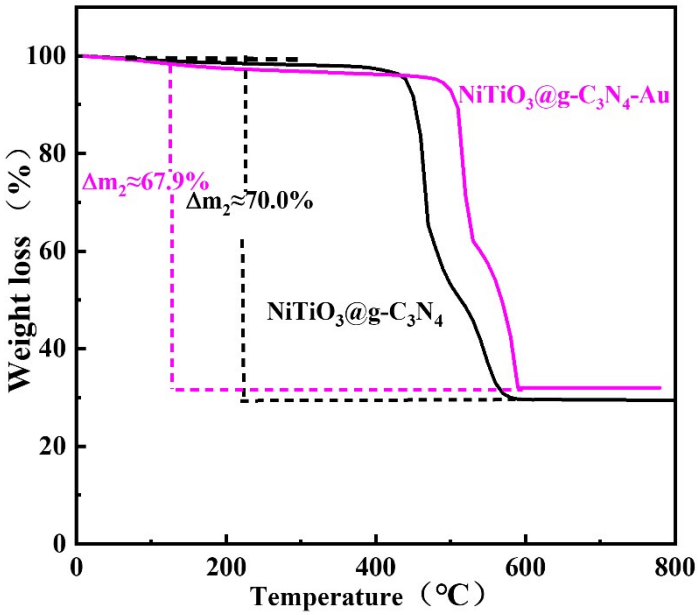

Fig.S4. TGA curves of the binary $NiTiO_3$@g-C_3N_4 NFs and ternary $NiTiO_3$@g-C_3N_4-Au NFs.

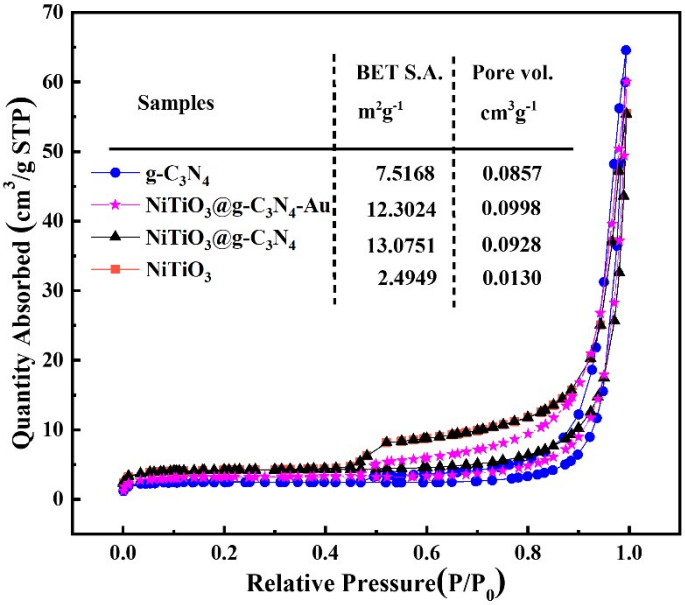

Fig.S5. BET Nitrogen adsorption/desorption isotherms of $NiTiO_3$ NFs, binary $NiTiO_3$@g-C_3N_4 NFs, ternary $NiTiO_3$@g-C_3N_4-Au NFs, and Pure g-C_3N_4; the inset shows the BET specific surface area and pore volume of samples.

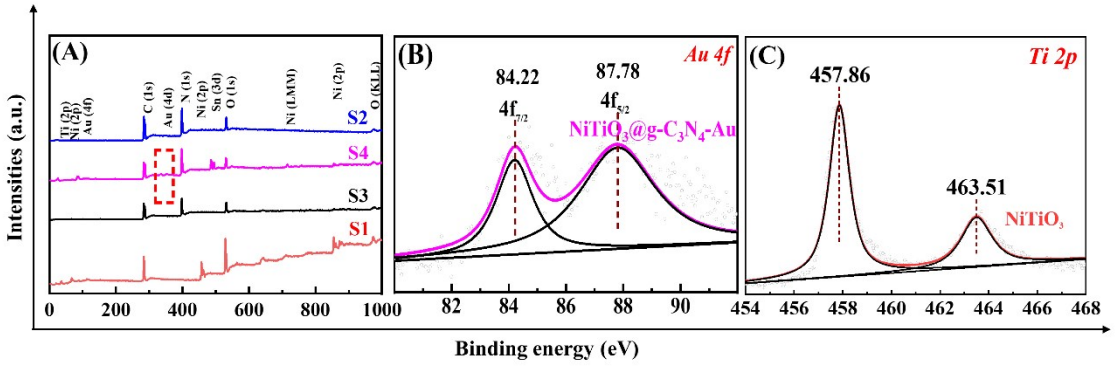

Fig.S6. (A) Fully scanned XPS spectra for the $NiTiO_3$ NFs, $NiTiO_3$@g-C_3N_4 NFs, $NiTiO_3$@g-C_3N_4-Au NFs and Pure g-C_3N_4; (B) high-resolution XPS spectra of Au 4f for $NiTiO_3$@g-C_3N_4 NFs Au NFs; (C) high-resolution XPS spectra of Ti 2p for $NiTiO_3$ NFs.

The C1s peak of 284.6 eV was used for XPS calibration.[1] For pure $NiTiO_3$ NFs, the Ni, Ti, and O signals appeared in the XPS survey spectrum in Fig. S6(A). As for $NiTiO_3$@g-C_3N_4 NFs and $NiTiO_3$@g-C_3N_4-Au NFs, these peaks of Ni, Ti, and O decreased remarkably due to the surface cover of g-C_3N_4 nanolayers. The survey spectra in Fig. S6(A) illustrated that the $NiTiO_3$@g-C_3N_4-Au NFs were composed of Ni, Ti, C, N, O, and Au, which was consistent with EDX result. The Au 4f spectrum of $NiTiO_3$@g-C_3N_4-Au NFs was shown in Fig. S6(B). The XPS peaks of Au $4f_{7/2}$ and Au $4f_{5/2}$ were presented at 84.22 and 87.78 eV, corresponding to metallic Au nanoparticles.

2.3

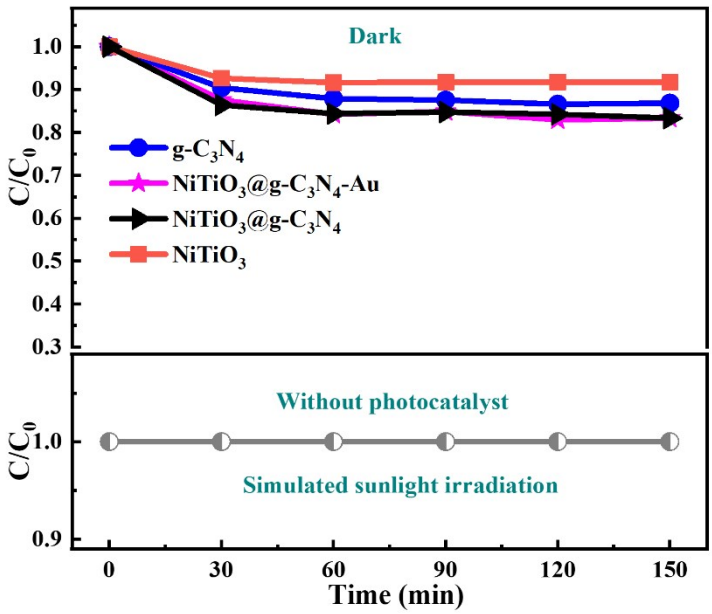

Fig.S7. Adsorption properties of different samples on RhB in the dark.

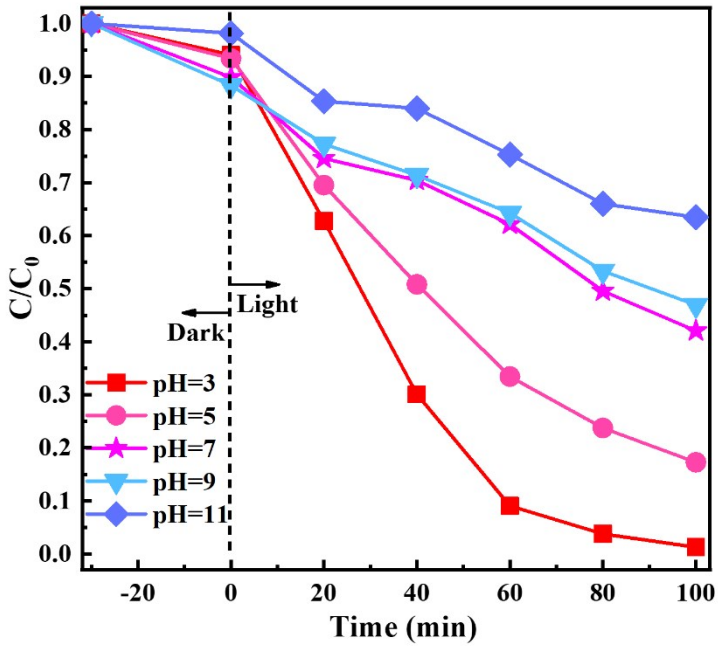

Fig.S8. Photocatalytic degradation of RhB for pure g-C_3N_4 under different pH environment HCl (pH = 3) and KOH (pH = 11) solution.

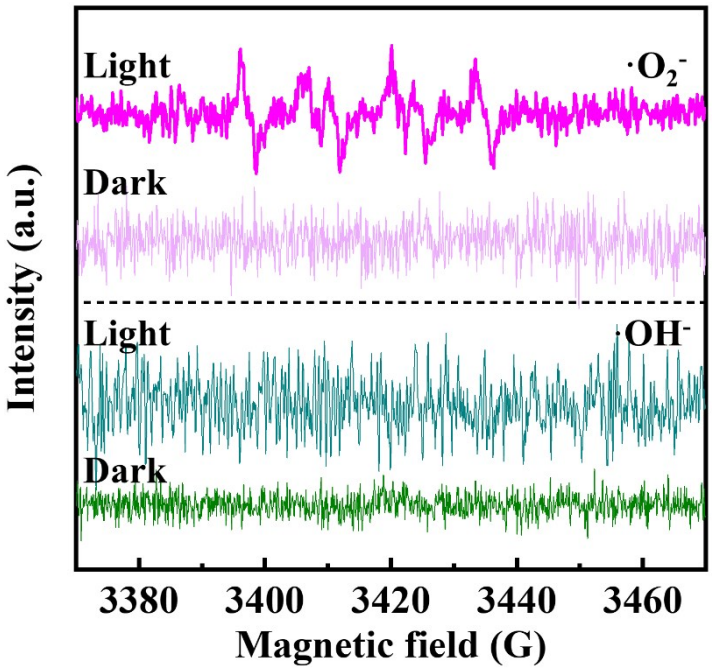

Fig.S9. EPR spectra of $NiTiO_3$@g-C_3N_4 NFs in the dark and light.

Reference

1. P. Thanh-Truc, S. G. Kang and E. W. Shin, Optical and structural properties of Mo-doped $NiTiO_3$ materials synthesized via modified Pechini methods, *Appl. Surf. Sci.*, 2017, **411**, 18-26.
2. T. F. Jaramillo, S. H. Baeck, B. Roldan Cuenya and E. W. McFarland, Catalytic activity of supported Au nanoparticles deposited from block copolymer micelles, *J. Am. Chem. Soc.*, 2003, **125**, 7148-7149.
3. H. Zhu, M. Du, M. Zou, C. Xu, N. Li and Y. Fu, Facile and green synthesis of well-dispersed Au nanoparticles in PAN nanofibers by tea polyphenols, *J. Mater. Chem.*, 2012, **22**, 9301-9307.